nature climate change

ARTICLES

https://doi.org/10.1038/s41558-020-00949-9

Climate change impacts on renewable energy supply

David E. H. J. Gernaat[1,2]✉, Harmen Sytze de Boer[1,2], Vassilis Daioglou[1,2], Seleshi G. Yalew[2,3,4], Christoph Müller[5] and Detlef P. van Vuuren[1,2]

Renewable energy resources, which depend on climate, may be susceptible to future climate change. Here we use climate and integrated assessment models to estimate this effect on key renewables. Future potential and costs are quantified across two warming scenarios for eight technologies: utility-scale and rooftop photovoltaic, concentrated solar power, onshore and offshore wind energy, first-generation and lignocellulosic bioenergy, and hydropower. The generated cost–supply curves are then used to estimate energy system impacts. In a baseline warming scenario, the largest impact is increased availability of bioenergy, though this depends on the strength of CO_2 fertilization. Impacts on hydropower and wind energy are uncertain, with declines in some regions and increases in others, and impacts on solar power are minor. In a future mitigation scenario, these impacts are smaller, but the energy system response is similar to that in the baseline scenario given a larger reliance of the mitigation scenario on renewables.

Renewable energy resources are becoming more important in the total primary energy supply. Currently, renewable resources supply 15% of the global primary energy[1]. Most of this is in the form of bioenergy (10%) and hydropower (3%), and the rest in other renewables (2%) such as photovoltaic (PV) and wind energy. Scenarios by the World Energy Outlook and integrated assessment models (IAMs)[1] estimate that, by 2040, renewables may supply 20–30% of the world's primary energy, and studies suggest it is theoretically possible to move toward a completely renewable energy system by 2050[2–6].

Since climate processes fuel most renewable energy resources, the impact of climate change on renewable energy supply has been identified as a key area for further research[7–18]. Many of the studies to date, however, have focused on either a specific region or technology. In addition, they do not typically account for uncertainty in physical climate change, and they tend to focus on the impact on energy potential rather than on energy systems more broadly. Here, we systematically assess the possible impact of climate change on renewable energy potential and the subsequent impact on global and regional energy systems under various climate change scenarios from four climate models.

We look at eight important renewable energy technologies for which methodologies to assess their technical and economic potential are well established: utility-scale PV[19,20], rooftop PV[21], concentrated solar power (CSP)[20], onshore wind energy[19], offshore wind energy[19], first-generation (sugars and vegetable oils) and second-generation (lignocellulosic) bioenergy[19,22] and hydropower[9]. For each of these resources, we re-estimate the technical and economic potential using methods described in literature for scenarios either with or without climate change. Using climate projections from general circulation models (GCMs) and Representative Concentration Pathways (RCP) scenarios (RCPs 2.6 and 6.0) available from the Inter-Sectoral Impact Model Intercomparison Project (ISIMIP2b)[23] database, we calculate future technical potential and combine this with economic information to form cost–supply curves that are used in IAMs. We then integrate these curves into the Integrated Model to Assess the Global Environment (IMAGE), an IAM, to study the implications for the energy system.

Climate and renewable energy potential

We use output from four GCMs (GFLD-ESM2M, HadGEM2-ES, IPSL-CM5A-LR and MIROC5; Supplementary Table 1) for the following climatic parameters: solar irradiance (kWh m^{-2} per day), temperature (°C), sugar cane and maize yields (t ha^{-1} yr^{-1}), wind speed (m s^{-1}) and runoff (kg m^{-2} s^{-1}) (see Supplementary Fig. 1 for maps of these variables during the historical period 1970–2000). As lignocellulosic crop yields (t ha^{-1} yr^{-1}) (switchgrass and *Miscanthus*, or trees) are not available in the ISIMIP2b database, they are computed here following the ISIMIP2b protocol. For each parameter, the model mean is calculated for the historical period and for 2070–2100 (see Fig. 1 for the difference between future and historical time periods under RCP6.0; see Supplementary Fig. 2 for RCP2.6). For each grid cell, a Wilcoxon signed-rank test was performed on two data series: (1) the historical data and (2) the future long-term (2070–2100) RCP data, to statistically test whether the mean ranks would differ (see dots in Fig. 1 and Data collection and development section).

The climate data were used as input to calculate renewable energy potential. Following the methodology described by Hoogwijk[19], this includes the theoretical potential, which is the upper limit of the resource availability based on biophysical conditions. For PV, for example, this is the total energy from solar irradiance on Earth in a year. In subsequent steps, this theoretical potential is constrained by geographical and technical restrictions. Geographical restrictions reduce the theoretical potential to areas considered available and suitable for energy production. For bioenergy, this means the exclusion of nature reserves, forests, water-scarce areas and areas used for agriculture. Similar restrictions are also applied to other

[1]PBL Netherlands Environmental Assessment Agency, The Hague, The Netherlands. [2]Copernicus Institute of Sustainable Development, Utrecht University, Utrecht, The Netherlands. [3]Faculty of Technology, Policy, and Management, Technical University of Delft, Delft, The Netherlands. [4]Wageningen Environmental Research, Wageningen University and Research, Wageningen, The Netherlands. [5]Potsdam Institute for Climate Impact Research, Member of the Leibniz Association, Potsdam, Germany. ✉e-mail: david.gernaat@pbl.nl

renewable technologies (see Renewable energy potential section). To the remaining geographical area, further technical restrictions are applied. Technical restrictions are conversion efficiencies that apply to the transformation of a primary to a secondary resource. For solar power and bioenergy potential, this is a simple conversion efficiency factor, but for wind energy and hydropower, this is calculated with power and flow duration curves (see Renewable energy potential section). The climate impacts were calculated for both the historical and future period using the ISIMIP2b database (see Supplementary Fig. 1). The differences between future and historical potential for all the renewable energy technologies under the RCP6.0 scenario are shown in Fig. 2. For bioenergy, impacts strongly depend on the uncertain strength of CO_2 fertilization (see Supplementary Text 1). Therefore, here results are shown with and without CO_2 fertilization for bioenergy.

The spatial patterns of most resources can be understood on the basis of the observed changes in climate parameters (for formulas, see Climate impacts on renewable energy section). In addition to direct changes in the primary resource (such as higher wind speeds leading to more wind power generation), there are also some indirect impacts, such as those of temperature on the efficiency of PV[24] and CSP[25] (higher ambient temperatures leads to lower solar cell efficiencies, see Climate impacts on renewable energy section). The relationship between precipitation changes and hydropower potential is more complex, as this calculation involves monthly discharge patterns. Hydropower plant design is subsequently influenced by complex optimization on the basis of those monthly patterns[9,26] (see Supplementary Fig. 3 for a graphical explanation). For wind energy, the optimization of hub height also affects the actual impacts.

For PV and CSP, the potential only changes modestly in most tropical areas, while there is a considerable increase in potential in more temperate regions, including the eastern United States, Europe and eastern China. The impacts for wind power are stronger and show a complex pattern across models. For hydropower, the change in potential directly maps onto changes in precipitation, with a clear decrease in Southern Europe and the southern parts of South America, Africa and Australia. An increase in hydropower potential is seen in Eastern Africa and India, among other places. For bioenergy, the results strongly depend on the inclusion of CO_2 fertilization, with an increase in potential in most regions with CO_2 fertilization and a decrease in most tropical regions without CO_2 fertilization. The CO_2 fertilization impacts on bioenergy are also regionally different, with boreal regions showing a stronger increase in bioenergy than tropical regions, which has implications for future supply chains and international trade.

The changes in potential, aggregated per technology, are summarized in Fig. 3 in both absolute numbers (EJ yr^{-1}) and relative difference (%). At the global scale, CSP (7.5 EJ yr^{-1}, 2.2%), rooftop PV (0.6 EJ yr^{-1}, 2.0%), first-generation bioenergy (5.8 EJ yr^{-1}, 32.4%), lignocellulosic bioenergy (45.9 EJ yr^{-1}, 38.1%) and hydropower (2.2 EJ yr^{-1}, 6.1%) show an increase in potential. The other technologies show a decrease: utility-scale PV (3.0 EJ yr^{-1}, 0.4%), offshore wind energy (8.6 EJ yr^{-1}, 2.1%) and onshore wind energy (22.1 EJ yr^{-1}, 4.1%). The uncertainty across different GCMs is especially large for hydropower and wind energy. Similar results for bioenergy are found in Haberl et al.[27], but in a sensitivity run without CO_2 fertilization, bioenergy potential shows competing signals—a mean decrease of 3% for first-generation biofuel but a mean increase of 3% in lignocellulosic bioenergy (see Fig. 3, indicated with red bars overlaid on bioenergy changes). The evidence for the CO_2 fertilization effect is discussed in Supplementary Text 1. The uncertainties are large and behave similarly to those around wind energy and hydropower, with ambiguity in the sign of change. RCP2.6 (Supplementary Fig. 5) shows lesser impacts, especially for bioenergy, for which the effect is roughly 40% less than the increase under RCP6.0. At this lower level of climate change, the results for solar PV, wind energy and hydropower are uncertain, with no clear signal in either direction.

Implementation in an integrated assessment model

The maps of technical potential, combined with economic information, are used to generate cost–supply curves. These curves show the cumulative technical potential against the production cost, showing that the cost of production in a given location depends on its productivity. Cost–supply curves are widely used in IAMs to model the long-term cost development of renewable energy technologies[28]. These curves present an indication of resource depletion, as the most productive sites are slowly being depleted and thus higher cost-incurring sites need to be used.

The cost–supply curves are implemented in IMAGE using the 30-yr average potential and costs for the nominal years 2000 (1971–2001), 2050 (2031–2071) and 2085 (2071–2100), with the climate input data as the only difference among the periods. For the years in between, the data are interpolated linearly with the exception of 2085–2100, during which the data are kept constant at 2085 levels. These data are used for the SSP2 baseline scenario (SSP2-RCP6.0) and SSP2 climate policy scenario (SSP2-RCP2.6), that is, with and without climate-impacted cost–supply curves for renewables (SSP2-RCP6.0-CI and SSP2-RCP2.6-CI) (Table 1). All other model inputs are kept the same, except the cost–supply curves. The SSP2 baseline scenario describes a world in which social, economic and technological trends follow a median trajectory, leading to additional radiative forcing by 2100 of around 6.5 W m^{-2} (ref. [29]) (note this is slightly higher than but close to the 6.0 W m^{-2} assumed in the ISIMIP2b protocol). The SSP2 climate policy scenario follows the same trends, but here policy is implemented to limit additional radiative forcing to 2.6 W m^{-2} by 2100, consistent with a warming of 2 °C with a 66% likelihood[29]. In the model, this is implemented with a global uniform carbon price combined with land-use policies[29,30], leading to a much higher contribution of renewable energy. See Supplementary Fig. 6 for details on scenario assumptions.

Climate impacts on the energy system

The energy system impacts under the baseline scenario, with and without climate impacts on renewables (SSP2-RCP6.0-CI and SSP2-RCP6.0, respectively) and with CO_2 fertilization, are presented in Fig. 4. The mean change (over the GCMs) in cumulative primary energy supply can be seen over the 2070–2100 period (Fig. 4a), along with the underlying uncertainty (Fig. 4c). Overall, the climate impact leads to a 4–6% higher renewable energy use. This is mostly due to bioenergy, with a 10–20% higher use in most model regions, further supported by the statistical significance test across

Fig. 1 | Multi-model mean change in climate patterns and yields determining renewable energy potential for RCP6.0. a–h, The difference between the multi-model mean (over GCMs GFLD-ESM2M, HadGEM2-ES, IPSL-CM5A-LR and MIROC5) of the historical period (1970–2000) and that of the future period (2070–2100) for solar irradiance (%) (**a**), temperature (%) (**b**), wind speed (%) (**c**), runoff (%) (**d**), sugar cane and maize yields with CO_2 fertilization (crop selected with highest biomass yield per cell per period) (%) (**e**), lignocellulosic crop yields (switchgrass and *Miscanthus*, or trees) with CO_2 fertilization (crop selected with highest biomass yield per cell per period) (%) (**f**), sugar cane and maize yields without CO_2 fertilization (crop selected with highest yield per cell) (%) (**g**) and lignocellulosic crop yields (switchgrass and *Miscanthus*, or trees) without CO_2 fertilization (crop selected with highest yield per cell) (%) (**h**). Black dots mark areas where the Wilcoxon statistical test shows significant ($P < 0.1$) differences across GCMs, compared with the historical situation. Note the different scales. See Supplementary Fig. 2 for RCP2.6.

GCMs (see Methods). The smallest impacts are seen in solar power, with hydropower and wind energy showing mixed results and large uncertainty ranges due to the spread among GCMs. The increase in renewable energy use leads to a decline in fossil fuel and nuclear energy use in most of the regions, resulting in a 1–2% reduction in cumulative CO_2 emissions (2015–2100). In a run without CO_2 fertilization, however, the energy system effect on bioenergy changes considerably (Fig. 4b). This panel shows bioenergy impacts from a separate baseline run without CO_2 fertilization (see Supplementary Fig. 7 for the full results from this run, and Supplementary Text 1 for a discussion on CO_2 fertilization). Assuming small or no CO_2 fertilization impacts leads to outcomes for bioenergy comparable to

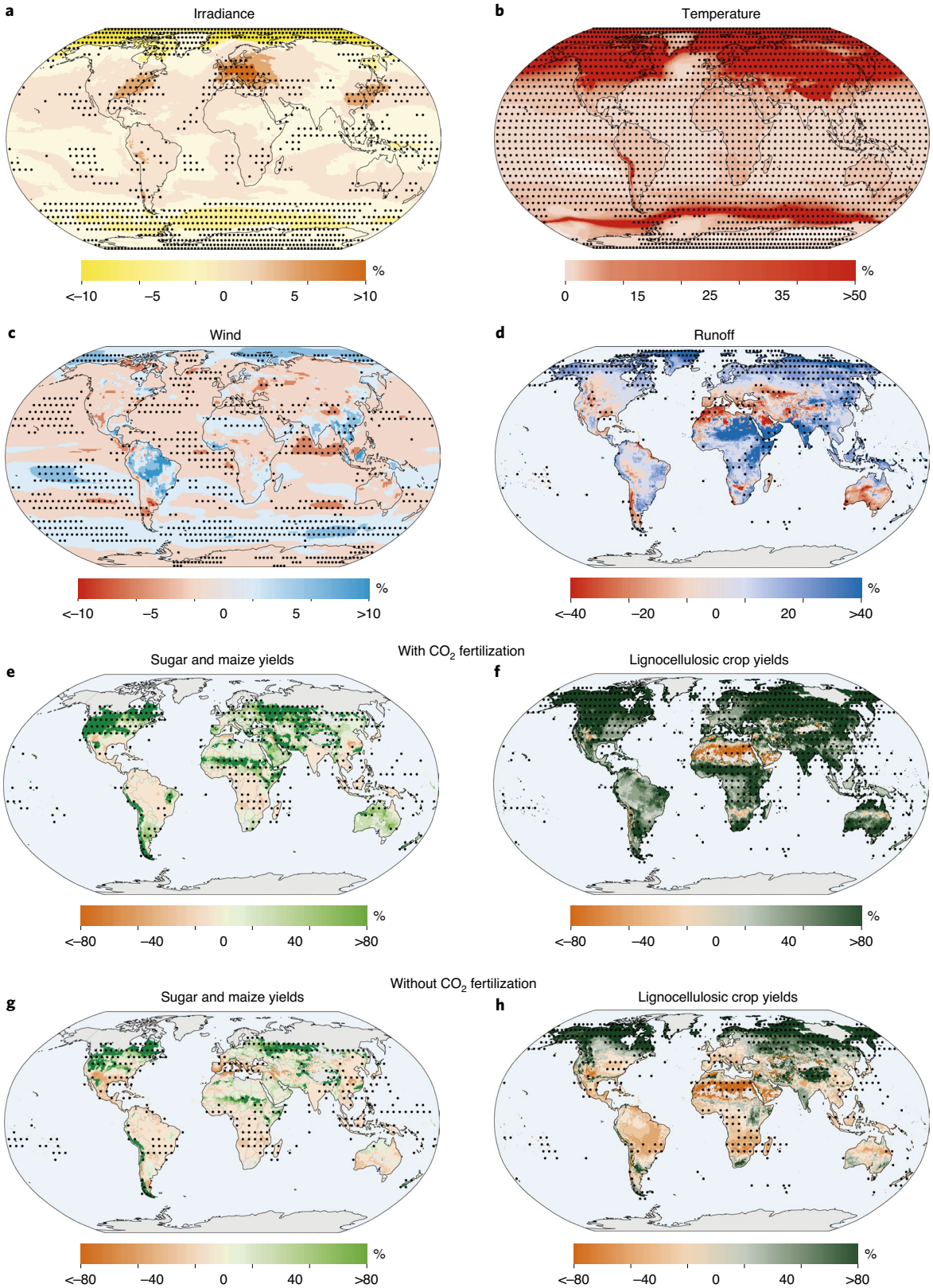

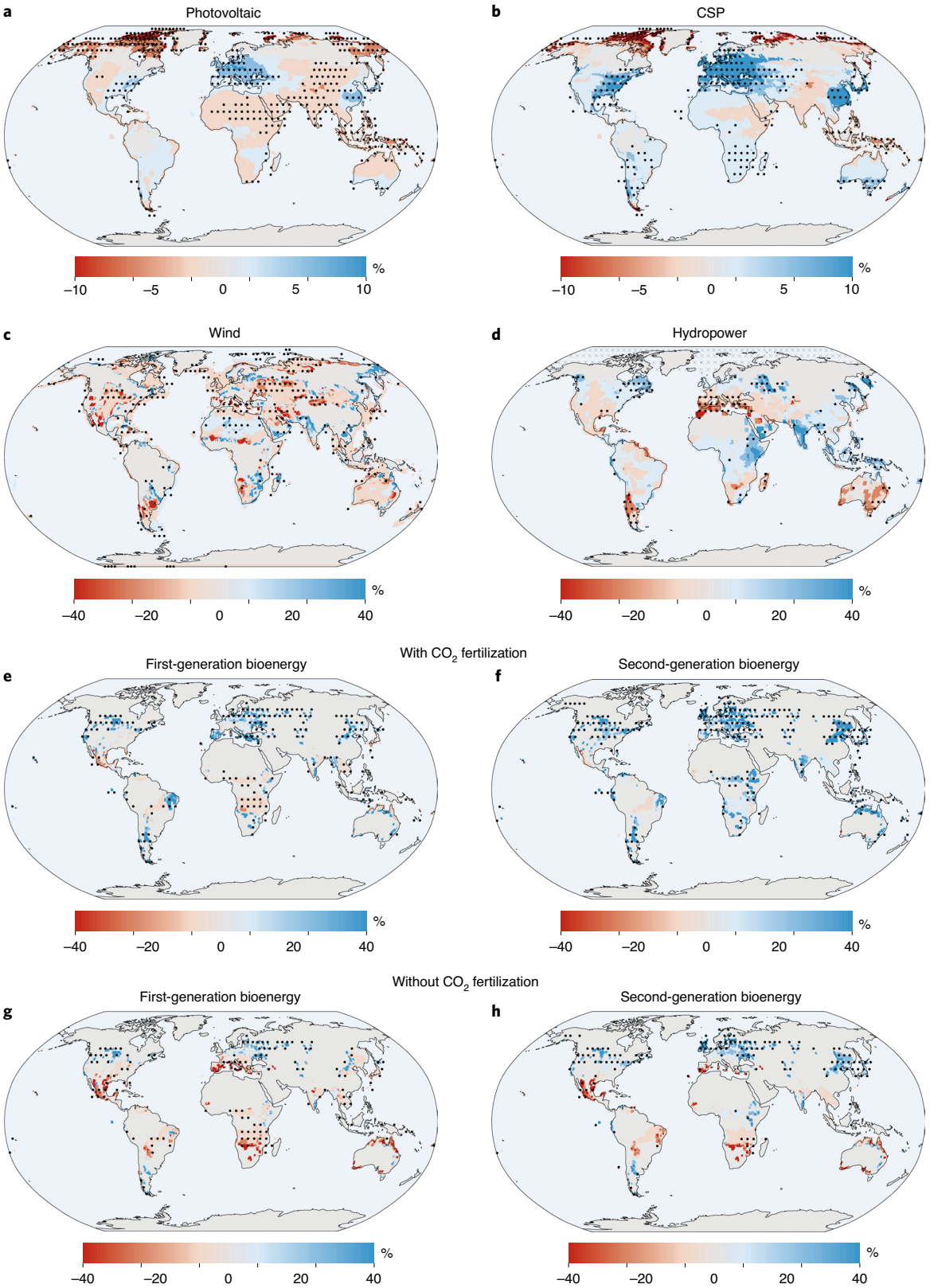

Fig. 2 | Multi-model mean change of technical potential under RCP6.0. a–h, The differences in the multi-model mean (over GCMs GFLD-ESM2M, HadGEM2-ES, IPSL-CM5A-LR and MIROC5) of the historical period (1970–2000) compared with the future period (2070–2100) for the renewable energy technologies considered in this study: (**a**) utility-scale and rooftop PV (**a**), CSP (**b**), onshore and offshore wind energy (**c**), hydropower (**d**), first-generation bioenergy with CO_2 fertilization (**e**), lignocellulosic bioenergy with CO_2 fertilization (**f**), first-generation bioenergy without CO_2 fertilization (**g**) and lignocellulosic bioenergy without CO_2 fertilization (**h**). Note the different colour bar scales among maps. Red represents a loss of potential, while blue shows an increase. Black dots mark areas where the Wilcoxon statistical test shows significant ($P < 0.1$) differences across GCMs compared with the historical situation. See Supplementary Fig. 4 for RCP2.6.

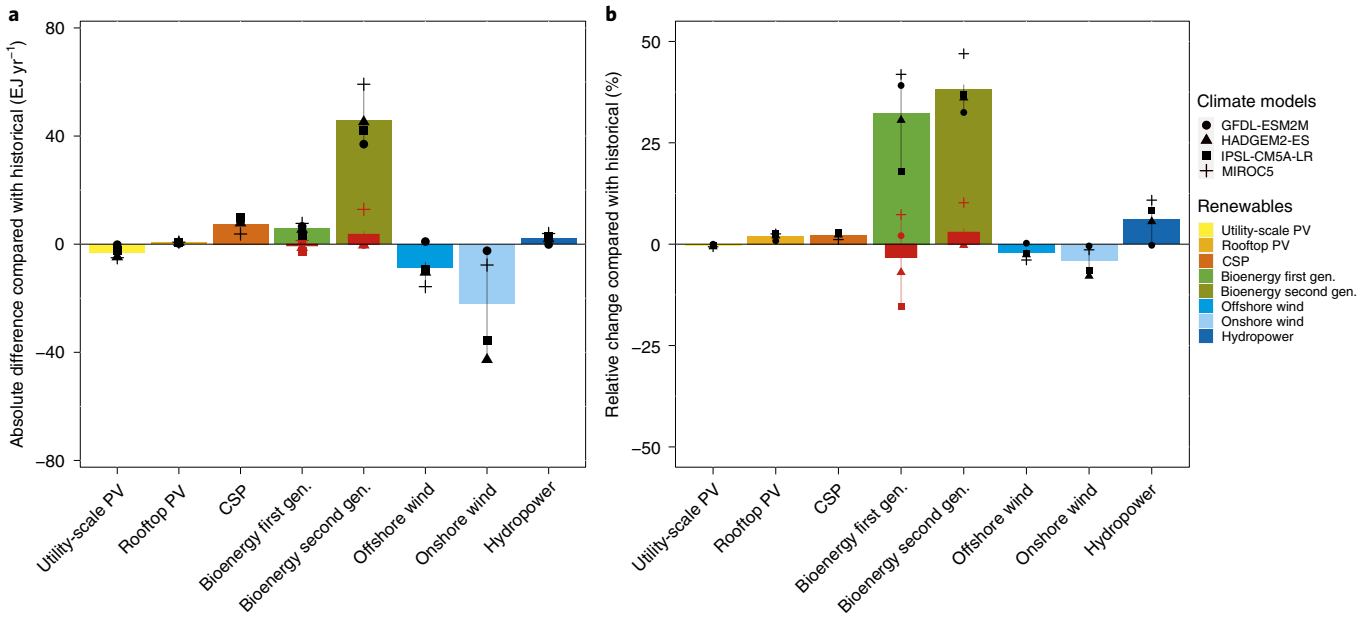

Fig. 3 | Global mean changes in technical potential for each renewable technology under RCP6.0. a, Absolute change in technical potential compared with the historical situation (EJ yr^{-1}). **b**, Relative change in technical potential compared with the historical situation (%) (same data as used in Fig. 2). Green bars for first- and second-generation bioenergy are for simulations with CO_2 fertilization; changes in bioenergy potential without CO_2 fertilization are overlaid as red bars. See Supplementary Fig. 5 for RCP2.6.

Table 1 | Scenarios with and without climate impacts on renewables

Scenario	Description
SSP2-RCP6.0	SSP2 baseline scenario without climate impacts on renewables. The climate component in the cost-supply curves, based on historical climate data, is kept constant throughout the run period.[a]
SSP2-RCP6.0-CI	Similar to the SSP2-RCP6.0 scenario, but with CIs on renewables. Cost-supply curves consistent with RCP6.0.[a]
SSP2-RCP2.6	SSP2 scenario that leads to 2.6 W m^{-2} in additional radiative forcing by 2100 (consistent with 2 °C) without climate impacts on renewables. The climate component in the cost-supply curves, based on historical climate data, is kept constant throughout the run period.
SSP2-RCP2.6-CI	Similar to the SSP2-RCP2.6 scenario, but with CIs on renewables. Cost-supply curves consistent with RCP2.6.

[a]The original IMAGE SSP2 scenario leads to 6.5 W m^{-2} in additional radiative forcing by 2100, which is slightly higher than the value of 6.0 W m^{-2} assumed in the ISIMIP2b database, but results are considered nearly compatible. Description of the scenarios used to generate cost-supply curves with the integrated assessment model in this study, where the climate component is either held constant during the simulation period or the climate impact (CI) is incorporated using RCP2.6 and RCP6.0 assumptions.

hydropower and wind energy: some regions (in Canada, Turkey and Southeast Asia) gain, while others (in South Africa, United States and Japan) lose.

The combined effect of all renewable climate impacts is shown in Fig. 4. This includes indirect effects (for example, reduced hydropower in Russia is an indirect effect of increased bioenergy). To unravel the direct effects, we use the climate-impacted cost–supply curves for each resource individually, meaning that the cost–supply curve of wind energy is used to calculate the impacts on wind energy (see Supplementary Fig. 8b for other renewables). This analysis confirms the clearly positive effect of bioenergy in most regions. Not including CO_2 fertilization, however, removes this positive effect entirely (Supplementary Fig. 7b), leaving a less robust and mixed signal. For hydropower, climate impacts lead to both gains and losses. In East Africa and Indonesia, hydropower increases significantly. Other regions that show less robust (not statistically significant) increases are North, South and West Africa, Japan and Indonesia. The regions that show a climate-change-induced decline in hydropower include Mexico, Central Asia, Central Europe, Oceania and Central America, though these signals are also not significant. Wind energy shows two regions (statistical significant signals) that increase by around 10%: Southeast Asia and Central Europe. Regions that decline in wind generation are Japan, which is statistically significant, and Korea, Mexico and Central America, which are not. The direct climate impacts on solar power are small (around 5%) yet robust. These effects are small because irradiation changes remain small and the negative effects of warming occur mostly at higher latitudes, which already have lower PV potential than low-latitude regions.

To unravel the indirect effects, we subtract the direct effects from the combined effect (Supplementary Fig. 8c). This shows that the increase in bioenergy use mostly leads to a decrease in fossil fuel and nuclear energy use, causing the CO_2 reduction discussed above. In some regions, the use of other renewables (mostly wind and solar power) also declines.

As part of a sensitivity analysis, we run the SSP2 scenario with higher shares of renewable energy (adapted from the high-renewables scenario in van Vuuren et al.[31]; Supplementary Fig. 6). The results from SSP2-RCP6.0-HRES with and without climate change are shown in Supplementary Fig. 9 (see also Supplementary Fig. 10 for SSP2-RCP2.6-HRES). The results show a similar pattern compared with the scenario with lower shares of renewables (SSP2-RCP6.0), such as increased bioenergy use. A notable difference, however, is that substitution effects occur mostly among renewables—a result that looks similar to those under SSP2-RCP2.6. Note, however, that more renewables lead to less emissions, likely resulting in less

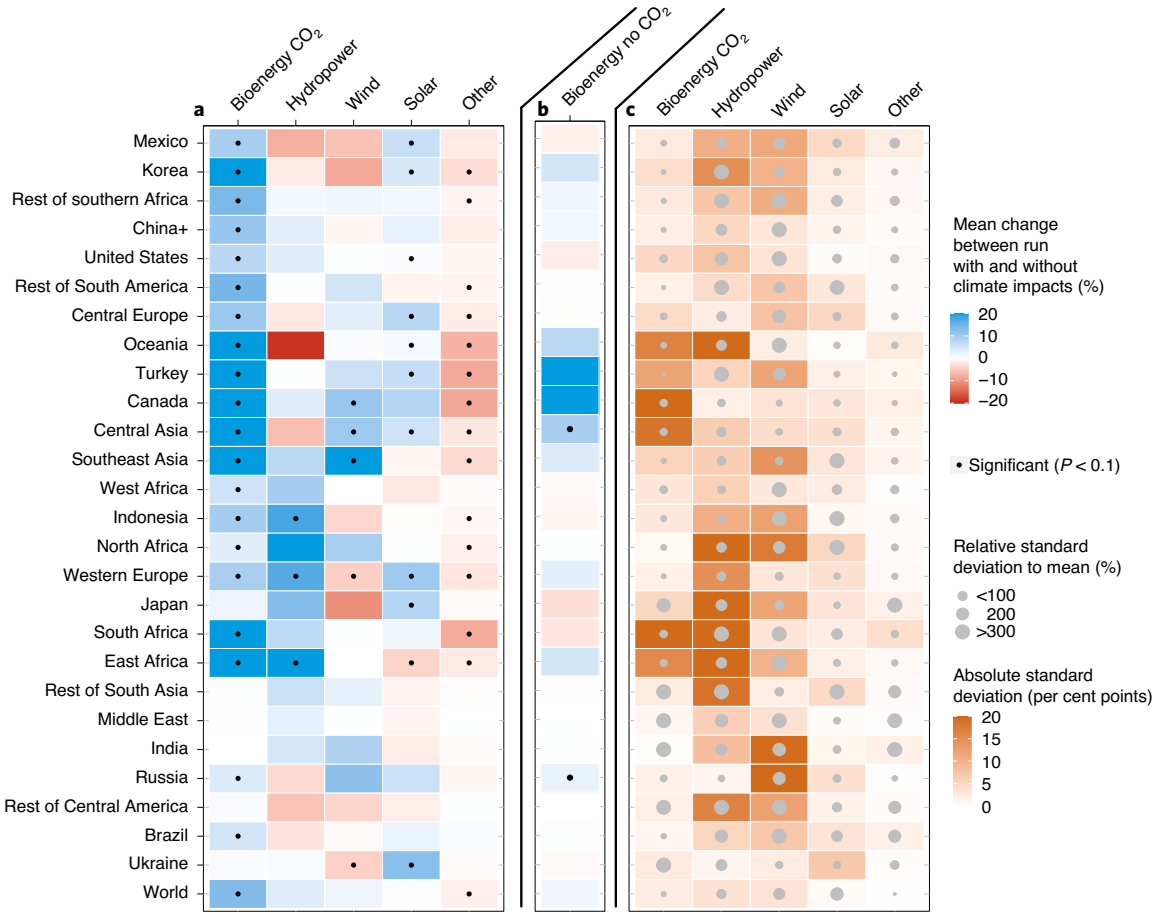

Fig. 4 | The combined relative effect of climate impacts on cumulative primary energy supply for each IMAGE model region. a–c, Comparison of SSP2-RCP6.0 scenario (without climate impacts on renewables) and SSP2-RCP6.0-CI (with climate impacts on renewables): multi-model mean change (over GCMs) of the cumulative primary energy supply in the 2070–2100 period per technology with CO_2 fertilization for bioenergy (**a**), mean specific climate impact on bioenergy without CO_2 fertilization (same data as used in Supplementary Fig. 7b) (**b**) and absolute standard deviation (per cent, shown in orange gradient) and the relative standard deviation (shown by grey dot size) over the GCMs of the data shown in **a** (**c**) **a**. Regions and technologies are ordered to form visual clusters of colour. China+ includes Taiwan. Black dots in **a**,**b** mark regions where Wilcoxon statistical test shows significant ($P < 0.1$) differences across GCMs, compared with the historical period.

climate change and smaller impacts on renewables (this scenario is therefore inconsistent with the RCP6.0 emissions budget).

The climate impacts on renewables under the SSP2-RCP2.6 scenario reveal interesting dynamics (Supplementary Figs. 11 and 12). Despite the lower impact on potentials due to limited levels of climate change (Supplementary Figs. 2, 4 and 5), the energy system effects are comparable to those under SSP2-RCP6.0. This is because the renewables account for a much larger share of the total energy system, making it more susceptible to small changes. There are, however, notable differences compared with SSP2-RCP6.0-CI. The first is the weaker impact of bioenergy, resulting from the smaller impact of CO_2 fertilization on the bioenergy potential. The second difference is that of the indirect effects (Supplementary Fig. 12c). SSP2-RCP6.0-CI shows that additional renewables lead to less fossil fuel use, whereas under SSP2-RCP2.6-CI, substitutions occur among renewables. Results from the RCP2.6 scenario need to be considered with care, however, given the lower degree of statistical significance and higher uncertainty across GCMs (Supplementary Figs. 2 and 4). Finally, we compare the SSP2-RCP6.0-CI total energy system cost with a hypothetical SSP2-RCP2.6-CI scenario to calculate the cost of inaction. Here, the former was 0.1% (0.02–0.16%) less expensive, leading to a minor financial gain.

Discussion

Our assessment represents an important step forward, as it includes climate impacts on a range of renewable energy technologies across various climate warming scenarios. Rather than providing a single impact assessment of one renewable technology, we therefore offer a systematic energy-system-wide evaluation of the most relevant renewables known today.

This study does have limitations. First, some climate impacts have been omitted, including the effect of direct irradiation on CSP and possible changes in the daily variation and extremes in temperature, wind speed and precipitation. In addition, the climate impact on residues used as feedstock for bioenergy have not been accounted for. Moreover, the climate impacts on fossil-fuel and nuclear-based electricity production (via cooling), electricity transmission, evaporation from reservoirs and fossil-fuel production (for example, on pipelines in Arctic areas) lie beyond the scope of this study. Higher water temperatures, for instance, can lead to cooling problems for thermal power production. Power stations might require relocation or the addition of more cooling towers, which could lead to additional cost. The impact of changes in climate extremes (such as weather events with values above or below normal) could be considerable[32]. Long periods of calm winds or drought, or reduced predictability of weather patterns, can be troublesome for energy

systems with a high share of renewables in the future. These periods may occur more frequently or intensely under climate change[33]. This paper focuses on long-term mean changes, partly because IAMs (designed to explore long-term global scenarios) are not able to use information on changing extremes or short-term events, and our impacts on renewable energy supply are therefore likely conservative. Climate extremes also affect fossil-fuel production however, which makes the net impact on renewable energy supply uncertain.

The study also shows the sensitivity of the results to including the CO_2 fertilization effect. While the existence of a fertilization effect is not uncertain, its strength is. The Lund–Potsdam–Jena managed Land (LPJmL) model—used here to create yield impacts—has a relatively strong fertilization impact, and in that light the two sets of results provided allow us to assess the impact of this uncertainty. We include a discussion on this in Supplementary Text 1.

Finally, we study the energy system impacts using one IAM, though these models are broad in focus and necessarily simplify their representation of the energy system. Repeating experiments using more models with varied representations of energy systems would advance our understanding of climate impacts on renewable energy. To aid in this development, all data presented in this paper are available (see 'Data availability') and may serve as input for various multi-model studies. Furthermore, our data can be valuable input for a broad range of follow-up studies that, for example, assess climate impacts on a local level or on economic/natural systems, or studies that assess cross-sectoral impacts involving the water–energy–climate nexus.

Climate change under a baseline warming scenario will impact renewable energy sources and future energy systems. At the global scale and over multiple decades, however, the risks are modest: a few percent more renewables and slightly lower CO_2 emissions. The strongest impact may be on bioenergy as a result of CO_2 fertilization, although the strength of this is uncertain. Also notable are the global yet less extensive impacts on CSP (increases) and wind energy (decreases). At regional scales, impacts can be much stronger, particularly for wind energy and hydropower potential. These findings may be important for future planning and regional energy system investment.

Online content

Any methods, additional references, Nature Research reporting summaries, source data, extended data, supplementary information, acknowledgements, peer review information; details of author contributions and competing interests; and statements of data and code availability are available at https://doi.org/10.1038/s41558-020-00949-9.

Received: 13 May 2019; Accepted: 15 October 2020;
Published online: 11 January 2021

References

1. IEA. *World Energy Outlook* (International Energy Agency, 2017).
2. Ram, M., et al. *Global Energy System based on 100% Renewable Energy – Power, Heat, Transport and Desalination Sectors* (Lappeenranta University of Technology and Energy Watch Group, 2019).
3. Jacobson, M. Z., Delucchi, M. A., Cameron, M. A. & Mathiesen, B. V. J. R. E. Matching demand with supply at low cost in 139 countries among 20 world regions with 100% intermittent wind, water, and sunlight (WWS) for all purposes. *Renew. Energy* **123**, 236–248 (2018).
4. Teske, S. *Achieving the Paris Climate Agreement Goals* (Springer, 2019).
5. Bogdanov, D. et al. Radical transformation pathway towards sustainable electricity via evolutionary steps. *Nat. Commun.* **10**, 1077 (2019).
6. Hansen, K., Breyer, C. & Lund, H. J. E. Status and perspectives on 100% renewable energy systems. *Energy* **175**, 471–480 (2019).
7. Turner, S. W. D., Hejazi, M., Kim, S. H., Clarke, L. & Edmonds, J. Climate impacts on hydropower and consequences for global electricity supply investment needs. *Energy* **141**, 2081–2090 (2017).
8. van Vliet, M. T. H., Wiberg, D., Leduc, S. & Riahi, K. Power-generation system vulnerability and adaptation to changes in climate and water resources. *Nat. Clim. Change* **6**, 375–380 (2016).
9. Gernaat, D. E. H. J., Bogaart, P. W., van Vuuren, D. P., Biemans, H. & Niessink, R. High-resolution assessment of global technical and economic hydropower potential. *Nat. Energy* **2**, 821–828 (2017).
10. Schaeffer, R. et al. Energy sector vulnerability to climate change: a review. *Energy* **38**, 1–12 (2012).
11. Mideksa, T. K. & Kallbekken, S. The impact of climate change on the electricity market: a review. *Energy Policy* **38**, 3579–3585 (2010).
12. Ciscar, J.-C. & Dowling, P. Integrated assessment of climate impacts and adaptation in the energy sector. *Energy Econ.* **46**, 531–538 (2014).
13. Chandramowli, S. N. & Felder, F. A. Impact of climate change on electricity systems and markets—a review of models and forecasts. *Sustain. Energy Technol. Assess.* **5**, 62–74 (2014).
14. Pryor, S. C. & Barthelmie, R. J. Climate change impacts on wind energy: a review. *Renew. Sustain. Energy Rev.* **14**, 430–437 (2010).
15. CCSP. *Effects of Climate Change on Energy Production and Use in the United States – Synthesis and Assessment Product 4.5* (US Climate Change Program, 2008).
16. Li, D. H. W., Yang, L. & Lam, J. C. Impact of climate change on energy use in the built environment in different climate zones—a review. *Energy* **42**, 103–112 (2012).
17. Emodi, N. V., Chaiechi, T. & Rabiul Alam Beg, A. The impact of climate variability and change on the energy system: A systematic scoping review. *Sci. Total Environ.* **676**, 545–563 (2019).
18. Yalew, S. G. et al. Impacts of climate change on energy systems in global and regional scenarios. *Nat. Energy* **5**, 794–802 (2020).
19. Hoogwijk, M. M. *On the global and regional potential of renewable energy sources* (Faculteit Scheikunde, Universiteit Utrecht, 2004).
20. Köberle, A. C., Gernaat, D. E. H. J. & van Vuuren, D. P. Assessing current and future techno-economic potential of concentrated solar power and photovoltaic electricity generation. *Energy* **89**, 739–756 (2015).
21. Gernaat, D. E., de Boer, H.-S., Dammeier, L. C. & van Vuuren, D. P. The role of residential rooftop photovoltaic in long-term energy and climate scenarios. *Appl. Energy* **279**, 115705 (2020).
22. Daioglou, V., Doelman, J. C., Wicke, B., Faaij, A. & van Vuuren, D. P. Integrated assessment of biomass supply and demand in climate change mitigation scenarios. *Glob. Environ. Change* **54**, 88–101 (2019).
23. Warszawski, L. et al. The inter-sectoral impact model intercomparison project (ISI–MIP): project framework. *Proc. Natl Acad. Sci. USA* **111**, 3228–3232 (2014).
24. Jerez, S. et al. The impact of climate change on photovoltaic power generation in Europe. *Nat. Commun.* **6**, 10014 (2015).
25. Crook, J. A., Jones, L. A., Forster, P. M. & Crook, R. Climate change impacts on future photovoltaic and concentrated solar power energy output. *Energy Environ. Sci.* **4**, 3101–3109 (2011).
26. ORNL. *New Stream-reach Development: A Comprehensive Assessment of Hydropower Energy Potential in the United States* (Oak Ridge National Laboratory, 2014).
27. Haberl, H. et al. Global bioenergy potentials from agricultural land in 2050: sensitivity to climate change, diets and yields. *Biomass Bioenergy* **35**, 4753–4769 (2011).
28. IAMC documentation contributors. *IAMC wiki* http://iamcdocumentation.eu/ (2018).
29. van Vuuren, D. P. et al. Energy, land-use and greenhouse gas emissions trajectories under a green growth paradigm. *Glob. Environ. Change* **42**, 237–250 (2017).
30. Doelman, J. C. et al. Exploring SSP land-use dynamics using the IMAGE model: regional and gridded scenarios of land-use change and land-based climate change mitigation. *Glob. Environ. Change* **48**, 119–135 (2018).
31. van Vuuren, D. P. et al. Alternative pathways to the 1.5 °C target reduce the need for negative emission technologies. *Nat. Clim. Change* **8**, 391–397 (2018).
32. Field, C. B., Barros, V., Stocker, T. F. & Dahe, Q. *Managing the Risks of Extreme Events and Disasters to Advance Climate Change Adaptation: Special Report of the Intergovernmental Panel on Climate Change* (Cambridge Univ. Press, 2012).
33. IPCC *Climate Change 2014: Impacts, Adaptation, and Vulnerability* (eds Field, C. B. et al.) (Cambridge Univ. Press, 2014).

Methods

Data collection and development. The overall methodology included calculating renewable energy potential and cost for the historical period and the future warming scenarios, implementing that information in an integrated assessment model (IAM) and quantifying the effect on the energy system.

Given the renewable energy technologies included, six inputs were collected from four GCMs (GFLD-ESM2M, HadGEM2-ES, IPSL-CM5A-LR and MIROC5): solar irradiance (kWh m^{-2} per day) (global horizontal), temperature (°C), wind speed (m s^{-1}), runoff (kg m^{-2} s^{-1}), sugar cane and maize yields (t ha^{-1} yr^{-1}) and lignocellulosic crop yields (switchgrass and *Miscanthus*) (t ha^{-1} yr^{-1}). These data, representing two Representative Concentration Pathways (RCPs) and averaged to three time periods (1971–2001, 2031–2071 and 2071–2100), were derived from the Inter-Sectoral Impact Model Intercomparison Project (ISIMIP2b) database[23] (see Supplementary Tables 1 and 2 for an overview showing which climate variables have an impact on which potential), except for the lignocellulosic crop yields, which were computed for this study following the ISIMIP2b protocol.

The data were available at 0.5° × 0.5° resolution, which is suitable for the calculation of all renewable energy potential except that of hydropower. The hydropower calculation requires discharges at 15″ × 15″ resolution, which was obtained by scaling down the low-resolution (0.5° × 0.5°) runoff maps and routing them using high-resolution (15″ × 15″) area accumulation and drainage direction maps from the HydroSHEDS project (see Gernaat et al.[9] for details on the routing methodology and scale-down).

Yields and runoff were both calculated by using the LPJmL global vegetation model[34,35]. Yields and runoff are indirect climate variables, because variables such as temperature, CO_2 concentration and precipitation are used as inputs to calculate changes in crop yields and runoff. Maize, sugar cane and lignocellulosic crops (switchgrass and *Miscanthus*) are C4 grasses without direct stimulation of photosynthesis under elevated atmospheric CO_2 concentrations (e[CO_2]), but they have water-saving benefits in dry regions. Trees are C3 plants and are thus subject to direct stimulation of photosynthesis under e[CO_2][36]. The evidence for the CO_2 fertilization effect is discussed in Supplementary Text 1. For each cell the crop with the highest yield was selected for bioenergy production. In most cells, however, grasses have larger yields and are therefore the most economic choice (Supplementary Fig. 13).

To assess the level of uncertainty, a Wilcoxon statistical test was performed. This test, like a *t* test, assesses whether the GCMs agree on the direction and magnitude of the change. For visual presentation in the maps, we summed values in an area of 5°×5° (100 cells) and applied the test to two data series: (1) historical data (1971–2001) and (2) long-term data (2071–2100) from the RCPs. If the test shows a significant ($P<0.1$) difference, this area is marked with a black dot (see, for example, Fig. 1). A similar test is performed on the IMAGE energy system results (see, for example, Fig. 4).

Renewable energy potential. The calculation of each renewable energy potential is explained in detail in separate published articles. Here, a short explanation is given introducing each.

Utility-scale PV and CSP start with the theoretical potential based on a global solar irradiation map (kWh m^{-2} per day)[20,37]. This is subsequently restricted by excluding unsuitable areas (for example, areas with permanent snow cover or steep mountainous terrain) to calculate the geographical potential (see Supplementary Table 3 for an overview on the suitability factors). The remaining area is further restricted by suitability factors. The idea behind suitability factors is that only part of the land is physically available for solar generation to ensure that it may keep the land-use function that it has, such as agricultural crop production. To calculate the technical potential, conversion efficiencies are assumed that are explained in Climate impacts on renewable energy section.

Rooftop PV builds on the method of utility-scale PV, using theoretical and technical aspects, but differentiates on the geographical potential[21,37]. For rooftop PV, the geographical potential is determined according to roof area. This area is estimated by dividing the living area per household by the number of floors per household, both of which are based on census data. The estimates distinguish between urban areas and rural areas and are combined with an urban/rural population map to scale down the estimated roof areas to grid level. The technical calculations are similar to those used to calculate utility-scale PV and are explained in Climate impacts on renewable energy section.

Calculations of onshore and offshore wind energy potential start with wind speeds (m s^{-1})[19,38,39]. Then, similar to the calculations for solar power, areas are excluded and further restricted according to suitability factors. For the remaining geographical area, based on wind data, the electricity output is calculated using a Weibull distribution function and power curve for the turbine. For details on the offshore wind methodology see Supplementary Text 2.

Bioenergy potential calculations start with primary biomass production, represented through yields (t ha^{-1} yr^{-1})[19,22,40]. Potential primary biomass sources include maize, sugar cane and lignocellulosic crops (switchgrass and *Miscanthus*, and trees). Land availability for bioenergy production is limited by agricultural production, following a 'food-first' principle where agricultural lands are determined first and are off limits for biomass production. The technical potential is further limited by excluding forests, nature reserves and water-stressed areas. In principle, bioenergy can be produced on remaining unprotected lands but also on abandoned agricultural lands. This technical potential is converted to several secondary energy carriers (solids, liquids, electricity and hydrogen) that compete in the energy system with other secondary energy carriers, such as fossil fuels or renewables (see Daioglou et al.[22] for a full description of biomass supply and demand in IMAGE).

Calculations of hydropower potential start with runoff (kg m^{-2} s^{-1}) that flows from high elevation to low elevation, representing discharge (see Data collection and development section for the routing methodology)[41,42]. On the basis of these discharge maps, >3.8 million site-specific hydropower installations were evaluated, at a 25 km interval for every river between 56° S and 60° N (the excluded area is due to unavailable topographic data). At each site, high-resolution topographic data (3″ × 3″) were used to calculate the cost-optimal dam dimensions and associated production potential. In this way, 60,000 suitable sites were identified, which together represent the remaining technical potential (see Gernaat et al.[9] for a full description of the site selection process).

The maps on technical potential for all renewables are combined with economic information to generate cost–supply curves. Assumptions on cost can be found in separate articles[9,19–22,38], but the general methodology is as follows: Each technology requires an investment before it can produce energy. The annualized (discount rate 10%; lifetime depends on technology considered) investment (in USD), including operation and maintenance cost, is divided by the expected annual production (kWh) to calculate the levelized production cost of energy (USD kWh^{-1}). This yields two global maps, namely a technical potential map (kWh) and a production cost map (USD kWh^{-1}). Together, these are used to generate a cost–supply curve by sorting (in ascending order) the cells in the production cost map while simultaneously adding the same cells from the technical potential map. For more information on the internal dynamics of the IMAGE model and how the cost–supply curves are implemented, see Supplementary Text 3.

Climate impacts on renewable energy. To assess how climate change affects renewable energy production, we needed to translate the climatic parameters into technical parameters. See Supplementary Table 2 for an overview on climate variables influencing technical potentials. Listed below are the key equations used to calculate the technical potential.

The technical potential for utility-scale PV ($E_{PV,i}$) for grid cell i (kWh yr^{-1}) is represented by

$$E_{PV,i} = I_i \times h \times A_i \times a_i \times \eta_{LPV} \times \eta_{PV} \times PR \quad (1)$$

where I_i is the solar irradiance (kWh m^{-2} yr^{-1}), h is the number of hours in a year (8,760), A_i is the available area suitable for PV (fraction depending on land use) (see Hoogwijk[19] for details), a_i is the area of cell i (m^2), η_{LPV} is the land-use factor or packing factor (0.47), η_{pv} is the PV panel efficiency corrected for atmospheric variables (see Eq. 3) and PR is the performance ratio expressing the difference between performance under standard test conditions and the actual output of the system due to losses from sub-optimal angles, as well as cable and inverter losses (85%)[43,44].

The technical potential for rooftop PV ($E_{RPV,i}$) for grid cell i (kWh yr^{-1}) is represented by[21]

$$E_{RPV,i} = I_i \times h \times hh_{i,u/r} \times FA_{hh,u/r} \times \beta \times S \times \eta_{PV} \times PR \quad (2)$$

where I_i is the solar irradiance (kWh m^{-2} yr^{-1}), h is the number of hours in a year (8,760), $hh_{i,u/r}$ is the number of urban and rural households per cell (based on the residential module in IMAGE and scaled down using a population map[45]), $FA_{hh,u/r}$ is the floor space per urban and rural household[45], β is the coefficient that converts the floor space as a fraction of the roof area, S (0.32) is the architecturally suitable area accounting for shading, orientation and architectural obtrusions (based on a study that used high-resolution satellite photos to assess available rooftop PV area in the United States[46]) and η_{PV} is the PV panel efficiency corrected for atmospheric variables (see Eq. 3).

The assumed PV panel efficiency (η_{Panel}) under standard test conditions was 17% (average in the current world market)[43,44]. This efficiency can, however, be changed by atmospheric variables, in particular, temperature[24,47,48]:

$$\eta_{PV} = \eta_{Panel} \times (1 + \gamma[T_i - T_{STC}]) \quad (3)$$

where η_{PV} is the PV panel efficiency corrected for atmospheric variables, η_{Panel} is the standard panel efficiency (17%), γ is $-0.005\,°C^{-1}$ (the typical efficiency response of monocrystalline silicon solar panels) and T_{STC} is 25 °C (the reference temperature in standard test conditions). T_i (°C) is modelled considering the effects of temperature, irradiation and wind:

$$T_i = c_1 + c_2 \times T_{ai} + c_3 \times I_i + c_4 \times V_i \quad (4)$$

where c_1 is 4.3 °C, c_2 is 0.943, T_{ai} is the ambient temperature (°C), c_3 is 0.028 °C m^2 W^{-1}, I_i is the solar irradiation (W m^{-2}), c_4 is -1.528 °C s m^{-1} and V_i is the surface wind velocity (m s^{-1}). If the ambient conditions T_{ai}, I_i and V_i result in a T_i of 25 °C

(similar to T_{STC}), the efficiency correction remains 1. If T_i is higher, however, the correction factor is less than 1 and thus reduces the panel efficiency (η_{Panel}).

The technical potential for CSP ($E_{CSP,i}$) for grid cell i (kWh yr^{-1}) equals[20]

$$E_{CSP,i} = I_i \times h \times A_i \times a_i \times \eta_{LCSP} \times \frac{\eta_{CSP}}{FLH_i} \quad (5)$$

where I_i is the solar irradiance (kWh m^{-2} yr^{-1}) with a minimum of 3 kWh m^{-2} per day, h is the number of hours in a year (8,760), A_i is the suitable area available for CSP (see Köberle et al.[20] for details), a_i is the area of cell i (m^2), η_{LCSP} is the CSP land-use or packing factor (0.37), η_{CSP} is the CSP efficiency corrected for atmospheric variables (see Eq. 6) and FLH_i is the full-load hour of a reference plant (parabolic through with a solar multiple 2) that depends on I_i.

The CSP efficiency (η_{CSP}) depends on the ambient temperature[25,49]. In a CSP plant, heat is captured by a solar collector and transported to a Rankine cycle turbine to produce electricity. The efficiency of the Rankine cycle (η_R) is assumed to remain static; the collector's efficiency (right-hand side of Eq. 6) depends on the ambient temperature:

$$\eta_{CSP} = \eta_R \times \left(k_0 - \frac{k_1 \times (T_f - T_{ai})}{I_i} \right) \quad (6)$$

where η_R is the Rankine cycle efficiency (40%), k_0 is 0.762, k_1 is 0.2125 W m^{-2} °C^{-1}, T_f is the temperature of the fluid in the absorber (the pipes where the mirrors focus the sunlight, assumed to be 115 °C), T_{ai} is the ambient GCM temperature and I_i is the GCM solar irradiation (W m^{-2}).

The technical potential for onshore and offshore wind energy ($E_{W,i}$) for grid cell i (kWh yr^{-1}) is represented by[19]

$$E_{W,i} = A_i \times \eta_a \times \eta_{ar} \times a_i \times D \times hf_i \quad (7)$$

where A_i is the suitable area available for onshore and offshore wind energy (for onshore wind energy, see Hoogwijk[19]; for offshore wind energy, see Supplementary Information S2), η_a is the annual availability of the wind turbine due to maintenance (95%), η_{ar} is the wind farm array efficiency (90%), a_i is the area per cell i (km^2), D is the power density (4 MW km^{-2}) and hf_i (h yr^{-1}) is the full-load hours (maximum 4000 h yr^{-1}), described by

$$hf_i = \alpha_1 \times Vh_i - \alpha_2 \quad (8)$$

where α_1 is 565 s h^{-1} m^{-1} yr^{-1}, Vh_i is the wind speed (m s^{-1}) at hub height (70 m) corrected for roughness length based on the land-use type (IMAGE data) and α_2 is 1745 kWh kW^{-1} yr^{-1} for the Weibull function with $k = 2$. This equation is based on data from turbine power curves assuming a cut-in wind speed of 4 m s^{-1} (minimum speed for power generation) and a cut-out wind speed of 8 m s^{-1} (maximum wind speed until the generator is turned off).

The technical potential for hydropower ($E_{H,j}$) at a location j (Wh yr^{-1}) is represented by[9]

$$E_{H,j} = \rho \times g \times DH_j \times QD_j \times h \times LFD_j \times \eta_{ww} \quad (9)$$

where ρ is water density (kg m^{-3}), g is gravitational acceleration (9.8 m s^{-2}), DH_j is the head of the dam (m), QD_j is the design discharge (see paragraph below) (m^3 s^{-1}), h is the number of hours in a year (8,760), LFD_j is the annual design load factor (see paragraph below) and η_{ww} is the water-to-wire efficiency (70%). This is a slightly simplified representation because the calculation involves two types of hydropower systems, one of which also includes pipe friction losses. Nevertheless, climate impacts for both systems occur in the same way and are described as such.

Climate impacts on hydropower depend on monthly runoff patterns. Monthly runoff from model simulations is routed along elevation-based flow direction routes to form monthly discharge patterns that are used, via flow duration curves, to determine the design discharge (QD_j) and design load factor (LFD_j). These factors regulate how much of the flow is used for hydropower and how much is spilled[9,26]. Because hydropower systems are designed to produce electricity at the lowest price and building dams is expensive, designers look for cost-optimal height and width, and they weigh the building costs against the revenues of electricity production. As a rule of thumb, this is determined by the monthly flow patterns and by selecting the fourth highest monthly flow[26]. This value is called the design discharge (QD_j) and directly determines the turbine output. Even though part of the annual flow spills (and thus some electricity production is lost), this is outweighed by the increased cost of building a higher dam. The fraction of the sum of the hours of maximum turbine output, compared with the total amount of hours, is the design load factor (LFD_j). See Supplementary Fig. 3 for a graphical illustration.

The technical potential for bioenergy ($E_{B,b,i}$) of type b (first-generation bioenergy or lignocellulosic bioenergy) and grid cell i (GJ yr^{-1}) is represented by[19,22]

$$E_{B,b,i} = Y_{b,i} \times A_{b,i} \times a_i \times MF_{b,R} \times \eta_{hv} \quad (10)$$

where $Y_{b,i}$ is the potential rainfed yield (t ha^{-1} yr^{-1}), $A_{b,i}$ is the suitable area available for bioenergy (fraction depending on land use), a_i is the area of cell i (ha^2), $MF_{b,R}$ is the management factor per IMAGE region representing agricultural management and technology[30] and η_{hv} are the heating values to convert tons of biomass into GJ (19.5 GJ t^{-1} dry for trees; 16.5 GJ t^{-1} dry for switchgrass and *Miscanthus*; 15.8 GJ t^{-1} dry for maize; 15 GJ t^{-1} dry for sugar cane).

Energy system modelling. The IMAGE energy system model (TIMER[50]; https://models.pbl.nl/image) was used to simulate the energy system response to climate change. The model simulates long-term trends in energy supply, conversion and demand through investments in and use of different types of energy carriers. These investment dynamics are subject to technology development and resource depletion, where technological development is implemented in the form of learning curves that decrease the production costs as a function of the cumulative capacity. On the other hand, resource costs increase as they get depleted, based on cost–supply curves (see Renewable energy potential section). The supply of energy is assumed to always meet the demand, and the decision to invest in additional capacity is based on the costs of energy production per technology, with larger market shares assigned to lower-cost options. Inputs to the model are macroeconomic scenarios and assumptions on technology development, preference levels and restrictions to fuel trade. Most modelled renewables produce electricity, except bioenergy. The electricity module simulates 28 different electricity generation combinations of renewable, nuclear, fossil fuel, and bioenergy electricity technologies. These technologies compete for a share in investments based on technology costs per amount of generated electricity (see Supplementary Tables 4 and 5 for technical and economic details). Cost data is based on International Energy Agency[51] and historical capacity numbers on International Renewable Energy Agency[52]. After the investment decisions, a merit order strategy determines the use of the technologies based on their operational costs, and an aggregated representation of system integration issues (calibrated to a detailed power model) is used to integrate intermittent supply into the system. Bioenergy is used as fuel in different parts of the energy system. Primary biomass is converted to solid fuels for the electricity sector, to liquid fuel for the transport sector and to feedstock for the non-energy industry sector, or as feedstock for hydrogen production. More information can be found in Supplementary Text 3.

Data availability

Source data are provided with this paper.

Code availability

The code that produced the renewable energy potentials and cost curves can be found at https://github.com/davidgernaat. PBL holds the proprietary rights to the IMAGE computer code; extensive documentation is provided (https://models.pbl.nl/image).

References

34. Gerten, D., Schaphoff, S., Haberlandt, U., Lucht, W. & Sitch, S. Terrestrial vegetation and water balance—hydrological evaluation of a dynamic global vegetation model. *J. Hydrol.* **286**, 249–270 (2004).
35. Bondeau, A. et al. Modelling the role of agriculture for the 20th century global terrestrial carbon balance. *Glob. Change Biol.* **13**, 679–706 (2007).
36. Beringer, T., Lucht, W. & Schaphoff, S. Bioenergy production potential of global biomass plantations under environmental and agricultural constraints. *GCB Bioenergy* **3**, 299–312 (2011).
37. Gernaat, D. *Scripts used to generate results presented herein* github.com/davidgernaat/Solar_CostCurves Version v1.0.0 (Zenodo, 2020); https://doi.org/10.5281/zenodo.4059441
38. Gernaat, D. E. H. J., van Vuuren, D. P., van Vliet, J., Sullivan, P. & Arent, D. J. Global long-term cost dynamics of offshore wind electricity generation. *Energy* **76**, 663–672 (2014).
39. Gernaat, D. *Scripts used to generate results presented herein* github.com/davidgernaat/Wind_CostCurves Version v1.0.0 (Zenodo, 2020); https://doi.org/10.5281/zenodo.4059451
40. Daioglou, V. & Gernaat, D. E. *Scripts used to generate results presented herein* github.com/davidgernaat/Bio_CostCurves Version v1.0.0 (Zenodo, 2020); https://doi.org/10.5281/zenodo.4059455
41. Gernaat, D. *Scripts used to generate results presented herein* github.com/davidgernaat/Hydro_CostCurves Version v1.0.1 (Zenodo, 2020); https://doi.org/10.5281/zenodo.4059487
42. Gernaat, D. *Scripts used to generate results presented herein* github.com/davidgernaat/Hydro_ClimateImpacts Version v1.0.0 (Zenodo, 2020); https://doi.org/10.5281/zenodo.4059453
43. Fraunhofer Institute. *Photovoltaics Report* (Fraunhofer Institute for Solar Energy Systems, 2018).
44. IRENA. *Renewable Power Generation Costs in 2017* (International Renewable Energy Agency, 2018).
45. Daioglou, V., van Ruijven, B. J. & van Vuuren, D. P. Model projections for household energy use in developing countries. *Energy* **37**, 601–615 (2012).

46. Gagnon, P., Margolis, R., Melius, J., Phillips, C. & Elmore, R. *Rooftop Solar Photovoltaic Technical Potential in the United States: A Detailed Assessment* (National Renewable Energy Laboratory, 2016).
47. Radziemska, E. The effect of temperature on the power drop in crystalline silicon solar cells. *Renew. Energy* **28**, 1–12 (2003).
48. Tonui, J. K. & Tripanagnostopoulos, Y. Performance improvement of PV/T solar collectors with natural air flow operation. *Sol. Energy* **82**, 1–12 (2008).
49. Dudley, V. *Test Results for Industrial Solar Technology Parabolic Trough Solar Collector* (Sandia National Laboratory, 1995).
50. van Vuuren, D. P. *Energy Systems and Climate Policy—Long-Term Scenarios for an Uncertain Future* (Utrecht University, 2007).
51. IEA. *World Energy Outlook* (International Energy Agency, 2019).
52. IRENA. *Renewable Capacity Statistics* (International Renewable Energy Agency, 2019).

Acknowledgements

A. Righart is acknowledged for editing part of the manuscript. The research leading to these results has received funding from EU's Horizon 2020 Navigate (no. 821124). We thank the JPI Climate initiative and participating grant institutes for funding the ISIpedia project.

Author contributions

D.E.H.J.G. and D.P.v.V. developed the idea. D.E.H.J.G. designed the experiments and wrote the manuscript. S.G.Y. managed all climate input data. C.M. conducted model simulations and provided bioenergy yield data. V.D. calculated the bioenergy potential. All authors discussed the results and contributed to the manuscript.

Competing interests

The authors declare no competing interests.

Additional information

Extended data is available for this paper at https://doi.org/10.1038/s41558-020-00949-9.

Supplementary information is available for this paper at https://doi.org/10.1038/s41558-020-00949-9.

Correspondence and requests for materials should be addressed to D.E.H.J.G.

Peer review information *Nature Climate Change* thanks Andre Lucena, Hannes Weigt and the other, anonymous, reviewer(s) for their contribution to the peer review of this work.

Reprints and permissions information is available at www.nature.com/reprints.

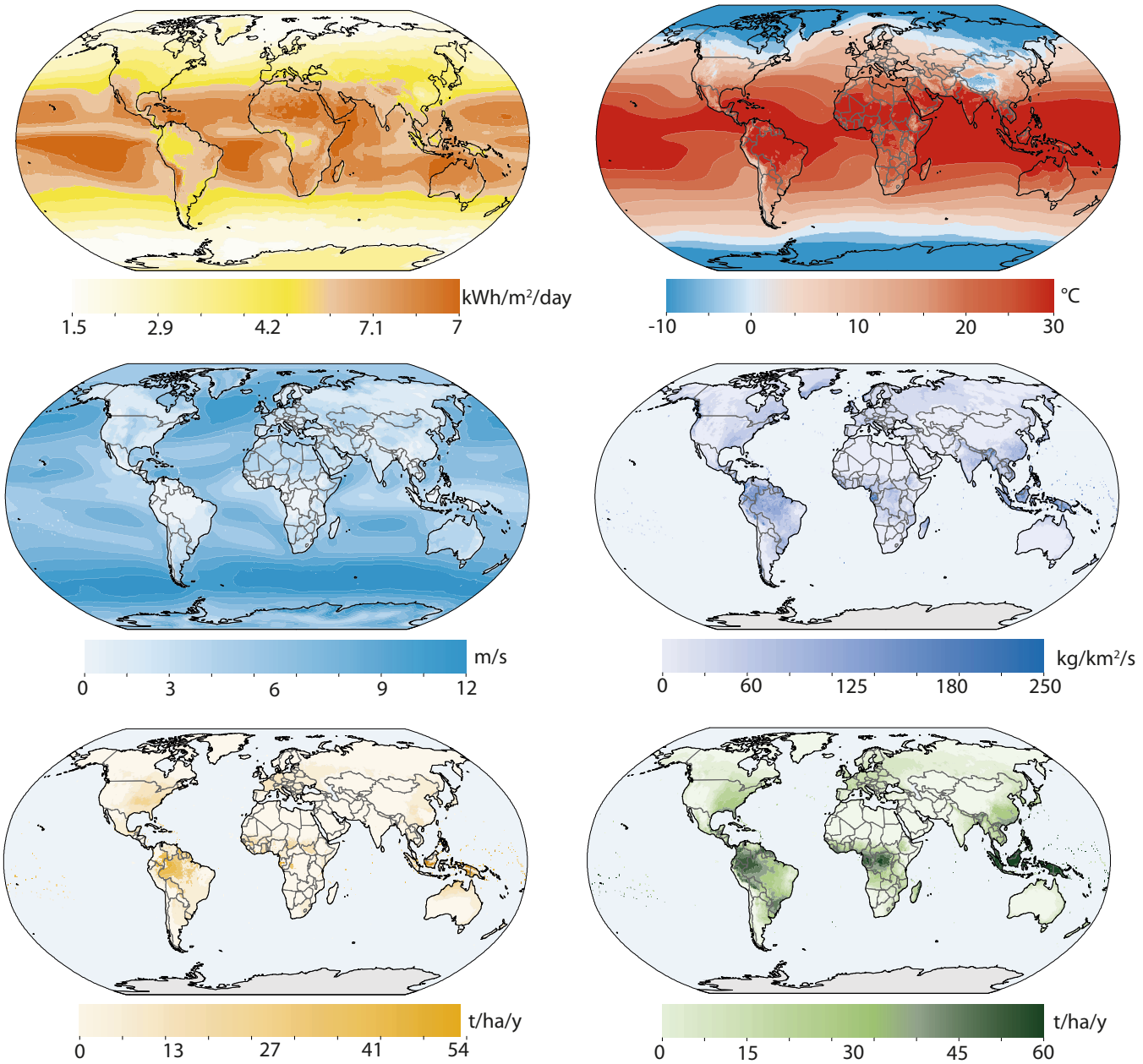

Extended Data Fig. 1 | GCM model mean for historical 30-year (1970–2000) average climate data used as input to calculate energy potentials. a, Solar irradiance (kWh m^{-2} day^{-1}) (global horizontal). **b**, Temperature (°C). **c**, Wind speeds (m s^{-1}). **d**, Runoff (kg m^{-2} s^{-1}). **e**, Sugar cane and maize yields (crop selected with highest yield per cell) (%). **f**, Lignocellulosic crop yields (switchgrass and Miscanthus, or trees) (crop selected with highest yield per cell) (%).

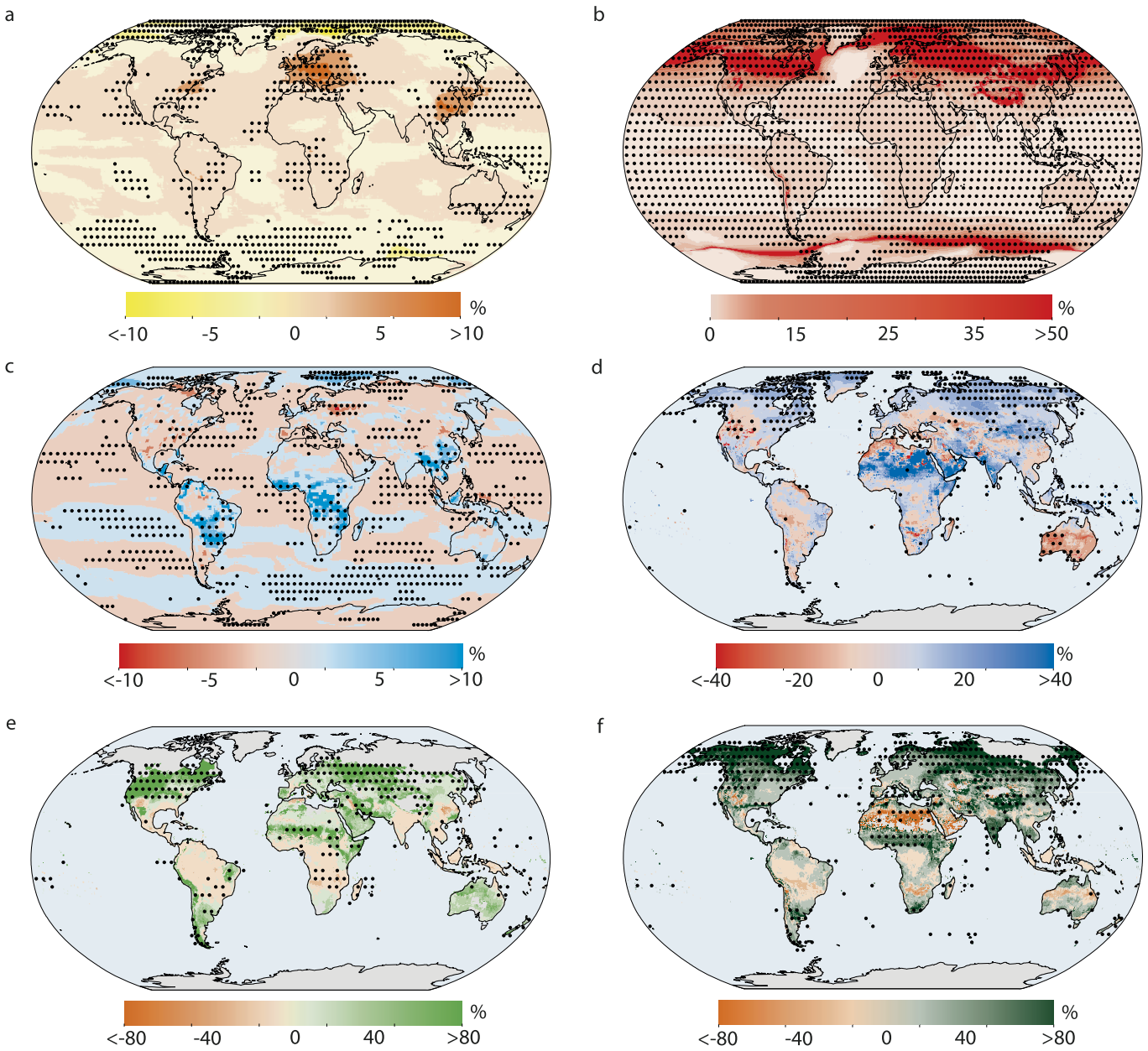

Extended Data Fig. 2 | GCM model mean change of climate patterns and yields in RCP2.6. a, solar irradiance (%) (global horizontal). **b**, temperature (%). (%). **c**, Wind speed (%). **d**, Runoff (%). **e**, Sugar cane and maize yields with CO_2 fertilisation (crop selected with highest yield per cell) (%). **f**, Lignocellulosic crop yields (switchgrass and Miscanthus, or trees) with CO_2 fertilisation (crop selected with highest yield per cell) (%).

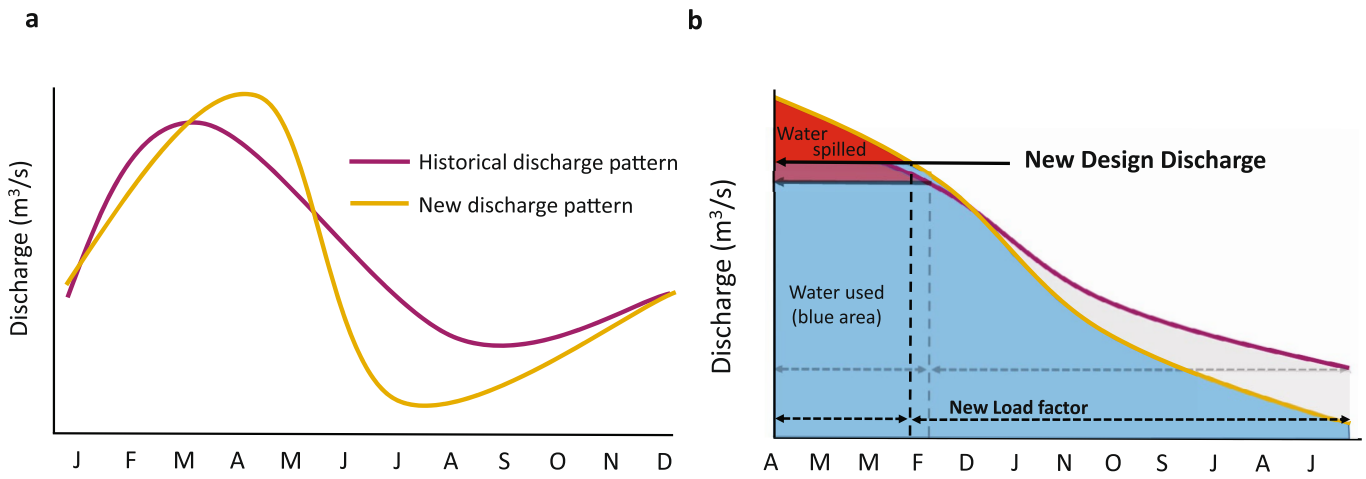

Extended Data Fig. 3 | Schematic illustration showing how climatic parameters can change the design discharge and load factors of a hydropower system. a, The purple line shows a typical historical discharge pattern at a hydropower location with a wet and dry season. The yellow line shows how new climate-change-induced precipitation patterns influence the discharge pattern, in this case with a wetter wet season and a prolonged dry season. Ordering the yellow line data into a flow duration curve, as illustrated in **b**, changes the design flow and design load factors. **b**, The flow duration curve with the new discharge pattern. The new discharge pattern (yellow line in **a**) forms a new flow duration curve with new design flow (defined as the fourth highest discharge month) and new design load factor (note that the months have shifted, too). The grey lines represent the old climate, the black lines illustrate the new.

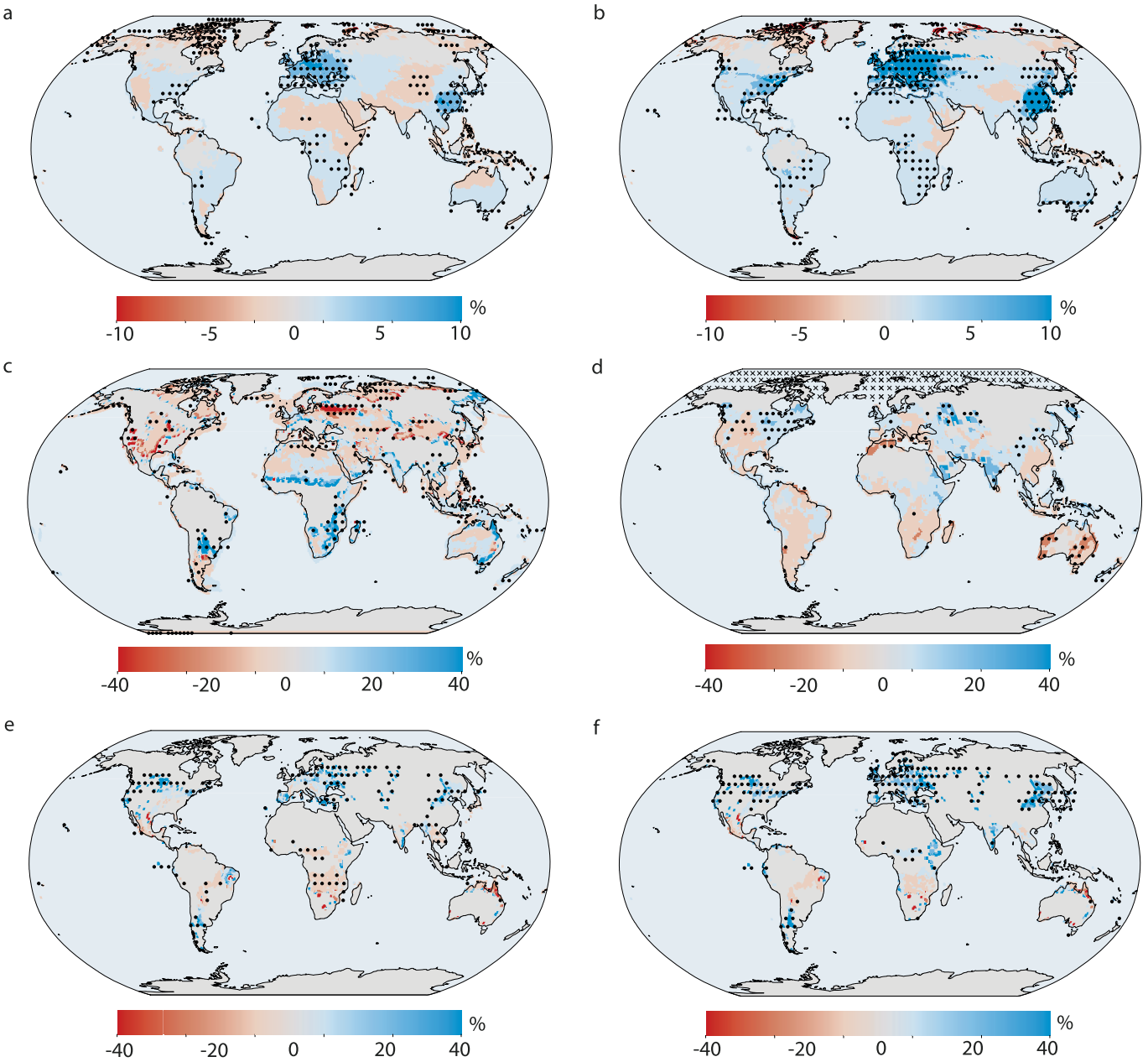

Extended Data Fig. 4 | Multi-model mean change of technical potential in RCP2.6. a, Utility-scale PV and rooftop PV. **b**, Concentrated Solar Power (CSP). **c**, Onshore and offshore wind energy. **d**, Hydropower. **e**, First-generation bioenergy with CO_2 fertilisation. **f**, Lignocellulosic bioenergy with CO_2 fertilisation.

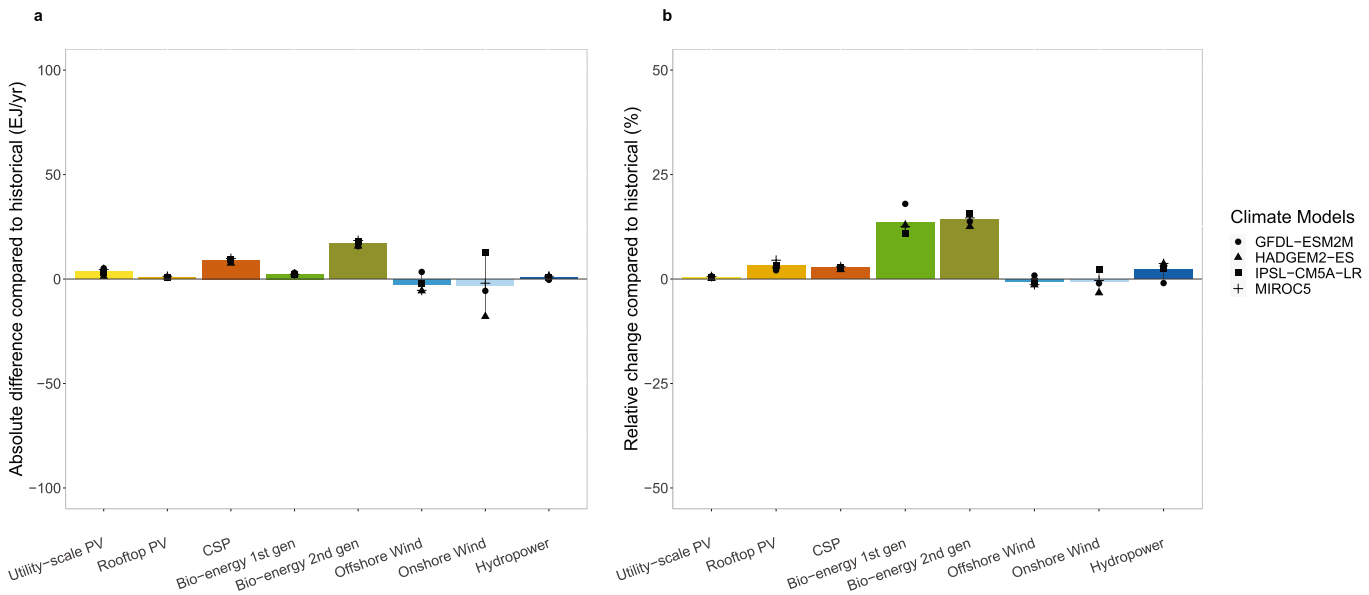

Extended Data Fig. 5 | The global mean changes in technical potential per renewable technology under RCP2.6. a, Absolute change in technical potential compared to the historical situation (EJ y^{-1}). b, Relative change in technical potential compared to the historical situation (%).

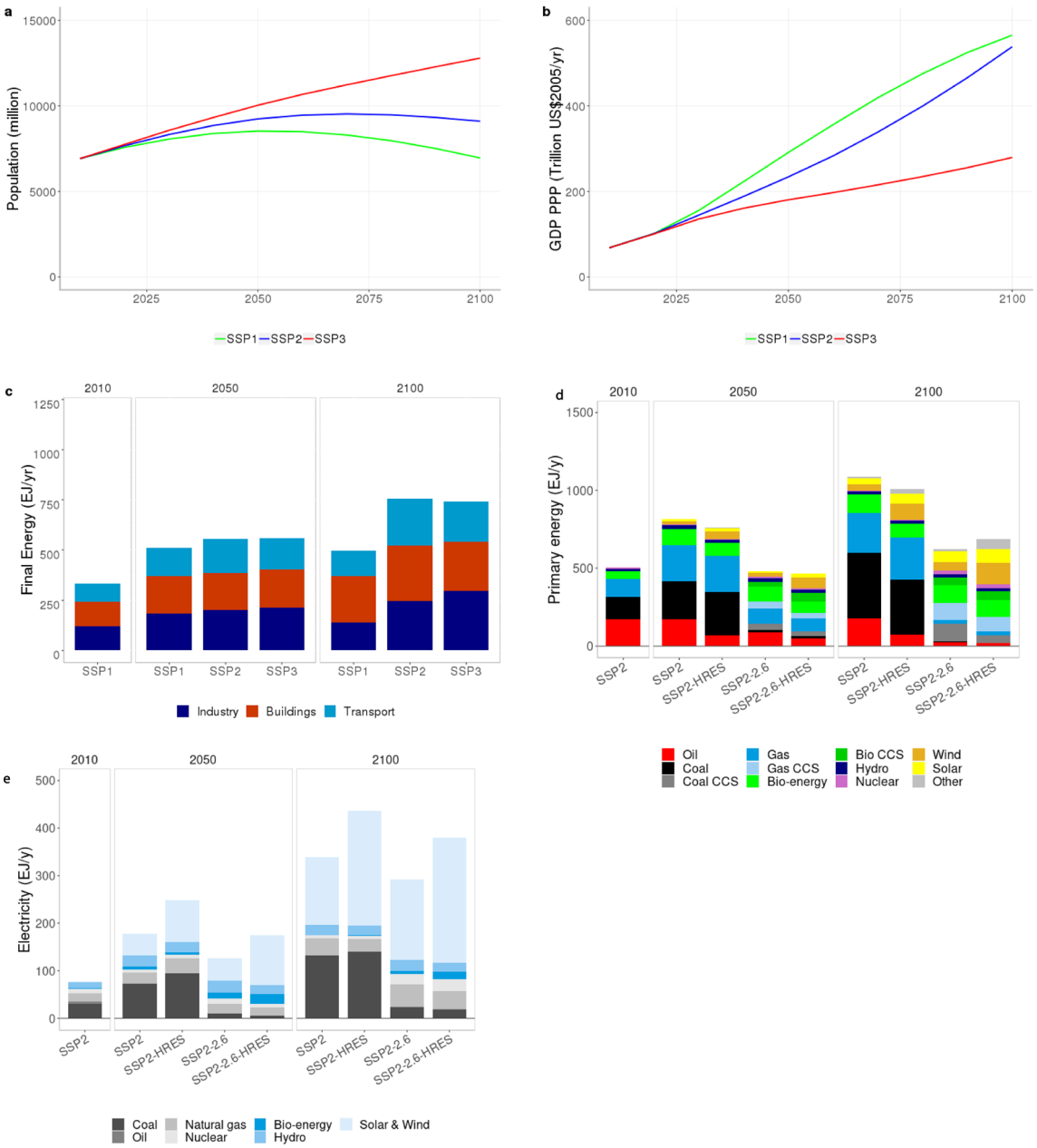

Extended Data Fig. 6 | Shared Socioeconomic Pathways (SSPs) assumptions for IMAGE. a, Global population (million) for SSP1-3. **b**, Economic development for SSP1-3 (GDP trillion USD_{2005} y^{-1}). **c**, Global final energy demand per sector for SSP1-3. **d**, Global primary energy use per energy carrier for SSP2 and SSP2-RCP26.

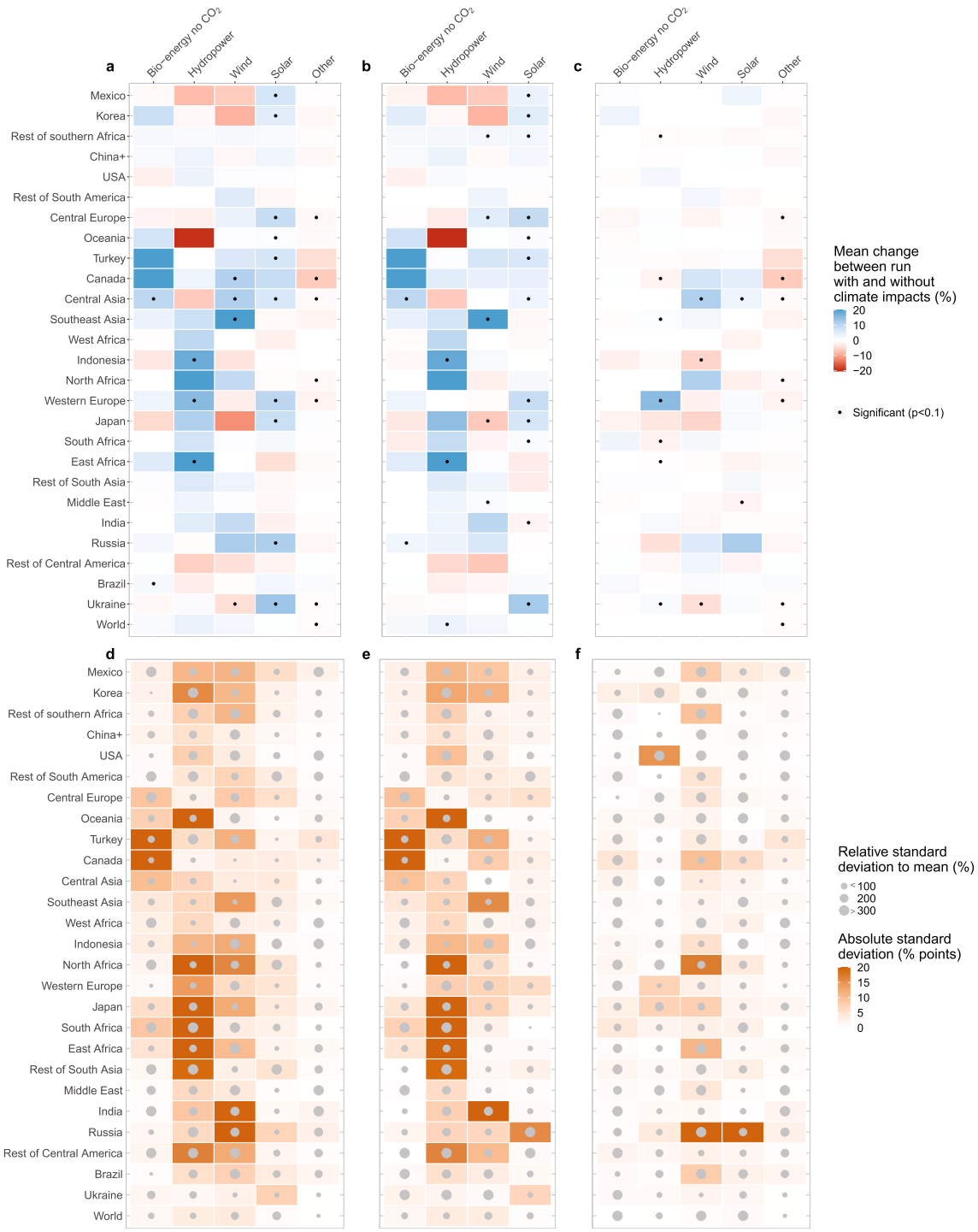

Extended Data Fig. 7 | The direct and indirect effect of climate impacts on cumulative primary energy in SSP2-RCP60-CI without CO_2 fertilisation (2070–2100). The top row shows the combined (**a**), direct (**b**) and indirect (**c**) mean change between a run with and without climate impacts on renewables in cumulative energy production (2070–2100) per technology group (%). The bottom row shows the uncertainty using the combined (d), direct (e) and indirect (f) absolute and relative standard deviation of the data shown in the top row.

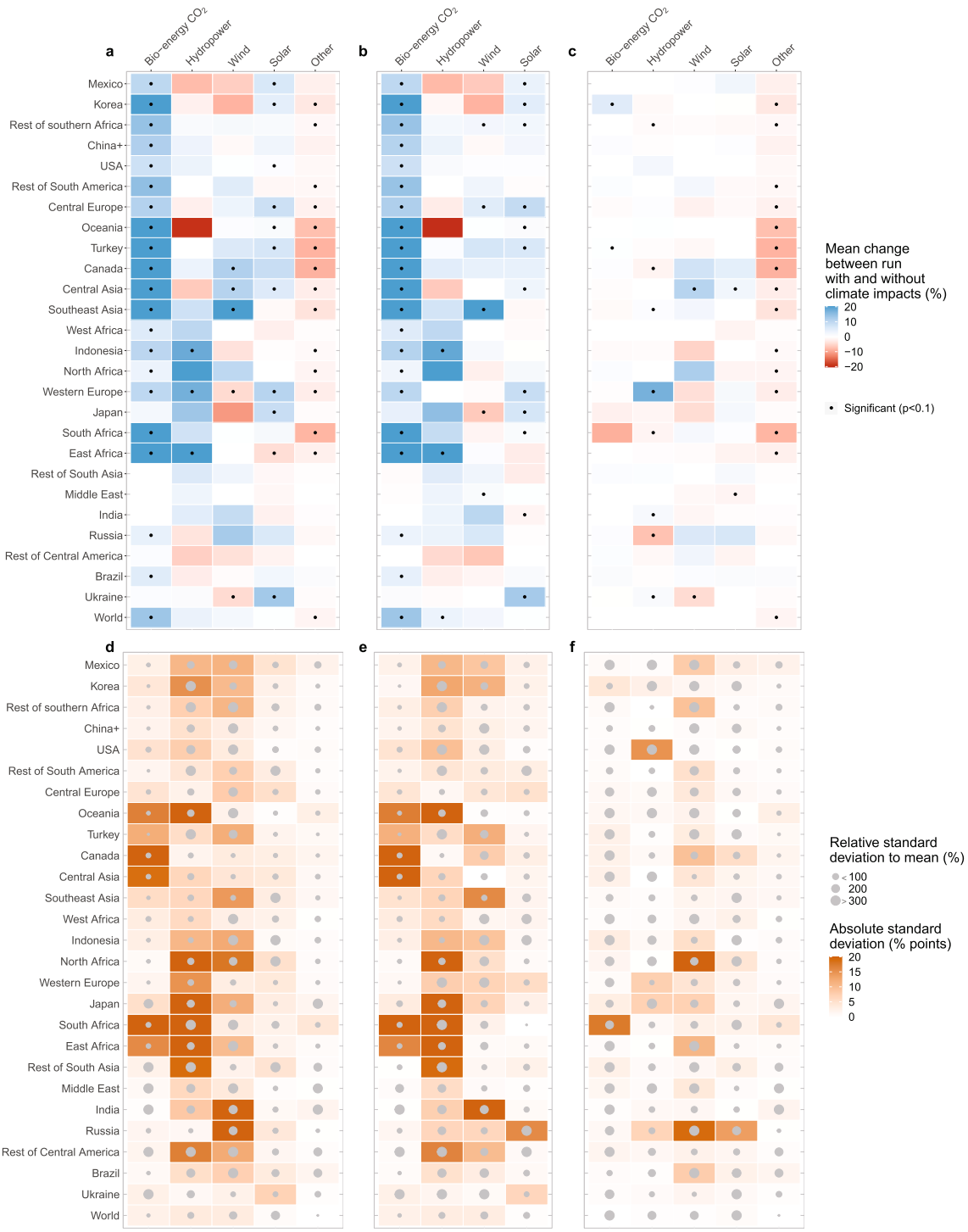

Extended Data Fig. 8 | The direct and indirect effect of climate impacts on cumulative primary energy in SSP2-RCP60-CI with CO_2 fertilisation (2070–2100). The top row shows the combined (**a**), direct (**b**) and indirect (**c**) mean change between a run with and without climate impacts climate impact in cumulative energy production (2070–2100) per technology group (%). The bottom row shows the uncertainty using the combined (**d**), direct (**e**) and indirect (**f**) absolute and relative standard deviation of the data shown in the top row.

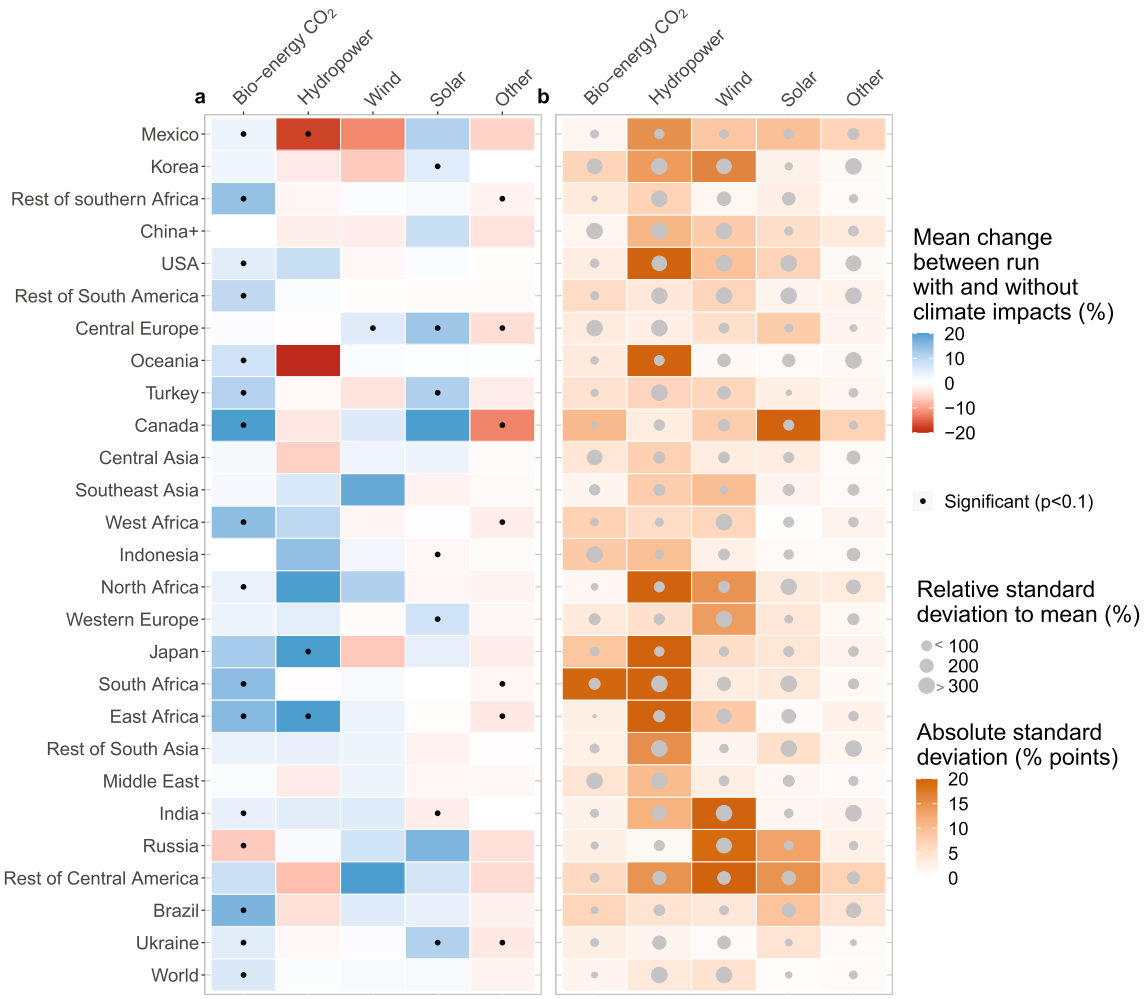

Extended Data Fig. 9 | The combined relative effect of SSP2-RCP60-HRES climate impacts on cumulative primary energy supply per IMAGE model region. a, The mean change (over the GCMs) of the cumulative primary energy supply in the period 2070–2100 per technology. **b**, The absolute (shown in orange gradient) and relative (shown in grey dot size) standard deviation of the data shown in a.

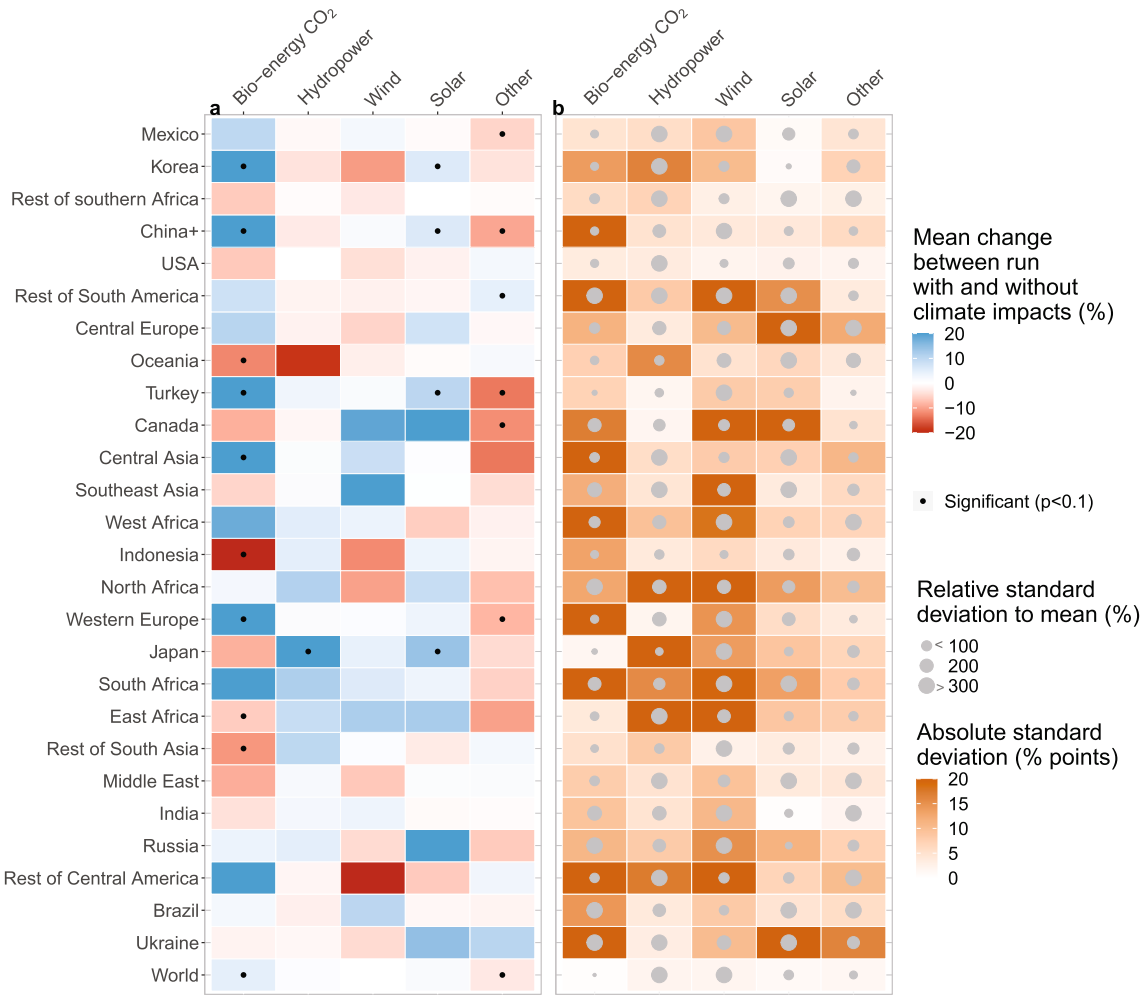

Extended Data Fig. 10 | The combined relative effect of SSP2-RCP26 climate impacts on cumulative primary energy supply per IMAGE model region. **a**, The mean change (over the GCMs) of the cumulative primary energy supply in the period 2070–2100 per technology. **b**, The absolute (shown in orange gradient) and relative (shown in grey dot size) standard deviation of the data shown in a.